JOURNAL OF GEOPHYSICAL RESEARCH, VOL. 93, NO. B7, PAGES 7943–7954, JULY 10, 1988

Modeling Surface Deformations at Complex Strike-Slip Plate Boundaries

VICTOR C. LI AND HUN SENG LIM

Department of Civil Engineering, Massachusetts Institute of Technology, Cambridge

Two new versions of the physical base-traction model of Li and Rice (1987) have been developed to study the loading processes and surface deformation near plate boundaries with geometric complexities, including a shallow creeping fault segment and two subparallel faults. Predictions of surface velocity and surface slip rate for the region between the San Andreas fault and the Pacific coast at the latitude of the Parkfield-Cholame segment using model parameters based on geologic, geodetic, and seismic considerations were found to be in good agreement with contemporary geodetic field data (not used in constraining model parameters). Also, predicted surface velocity for the Salton Sea-Coachella Valley area were fit to recently derived contemporary geodetic data and very large baseline interferometry data, although here the model parameters are not well constrained.

INTRODUCTION

Certain sections of the San Andreas fault do not exhibit a uniform geometry of a single fault strand which is locked from the surface to a certain depth. The geometric complexities could include adjacent subparallel faults, branch faults, and shallow surface creeping zones. A model containing a simple single-fault geometry clearly cannot account for the presence of these physical features. *Prescott et al.* [1979], *King and Savage* [1983], and *Prescott and Yu* [1986] have attempted to model adjacent subparallel faults using dislocation models involving slip at depth at the location of each of the active faults. *King et al.* [1987] modeled shallow creep behavior using a dislocation model involving a uniform slip rate from the surface to a certain depth below which a different deep slip rate is imposed. These simple kinematic models are quite successful in reproducing the asymmetric nature of surface deformation in the presence of subparallel faults or slip discontinuity on the fault trace in the presence of surface creep. However, they do not provide a basis for forward (in time) modeling of the evolving deformation processes because of the kinematic nature. Moreover, tectonophysical interpretation of constrained kinematic model parameters cannot be made too literally because of the nonphysical nature of imposed slip distribution (J. R. Rice et al., Dislocation modeling of surface deformation rate near a strike-slip plate boundary, submitted to *Journal of Geophysical Research*, 1988, hereinafter referred to as submitted manuscript, 1988).

In this paper, we present an extension of a model developed by *Li and Rice* [1987]. This physically motivated model takes into account the mechanical coupling between the elastic lithosphere and viscoelastic asthenosphere which allows the study of both the spatial variation with distance from the fault trace as well as the time dependence over a complete earthquake cycle of the surface deformation rates. The model incorporates a plausibly realistic long-term driving mechanism of steady upper mantle flow consistent with the geologically estimated rate for the San Andreas fault system. The seismogenic zone is assumed to undergo periodic earthquakes with slip magnitude and periodicity compatible with the plate velocity. A particular feature of the Li-Rice model is that the deep aseismic slip motion is obtained as a calculated response (based on assumed nonelastic constitutive behavior) rather than an imposed motion as is the case with kinematic models. The Li-Rice model produces whole-cycle surface strain rate consistent with geodetic data assembled by *Thatcher* [1983] for the San Andreas fault and also predicts velocity profiles (station velocity versus distance from the San Andreas) consistent with contemporary geodetic data from the Palmdale area [*King and Savage*, 1984; *McGarr et al.*, 1982; M. Lisowski and J. C. Savage, personal communications, 1987].

The original version of the base-traction model (so called because stress and motion is transmitted to an elastic middle and upper crust through a viscously relaxing asthenospherelike lower crustal layer by steady upper mantle motion) by *Li and Rice* [1987] considers a single fault with a locked zone extending from the surface to a certain depth below ground surface. This geometry adequately describes the condition at certain locations along the San Andreas fault where geodetic and seismicity data suggest that the fault is composed of a single major strand with no surface creep. However, other locations along the San Andreas fault exhibit different physical features.

The section of the San Andreas fault near Cholame southeast of Parkfield is in the transition zone between the central creeping section and the southern locked section of the fault (Figure 1). In addition to deep aseismic motion inferred to occur below the locked zone, shallow creep behavior has been detected here [*Burford and Harsh*, 1980; *Schulz et al.*, 1982; *King et al.*, 1987].

Along certain sections of the San Andreas fault, there exists a number of subparallel faults running adjacent to the main San Andreas fault. These faults include the San Jacinto and Elsinore fault in the Salton Sea area in southern California (Figure 1). The subparallel faults may interact and distort the surface deformation profile from that associated with a single major fault [*King and Savage*, 1983].

In this paper, by specific modeling of the plate boundary geometry, we extend the Li-Rice base-traction model to incorporate the two physical features described above. Based on independent data sets for constraining model parameters, predictions of surface velocity and surface creep rate are generated for the Cholame-San Luis Obispo area. Reasonable agreement with trilateration data [*King et al.*, 1987] is obtained. The repeated line length observations for the San Luis network has been made by the California Department of Water Resources in the 1970s and by the U.S. Geological Survey in the 1980s. For the geodetic data from the Salton Sea network (M. Lisowski and J. C. Savage, personal communicating, 1988) and very long baseline interferometry (VLBI)

Paper number 7B2071.
0148-0227/88/007B-2071$05.00

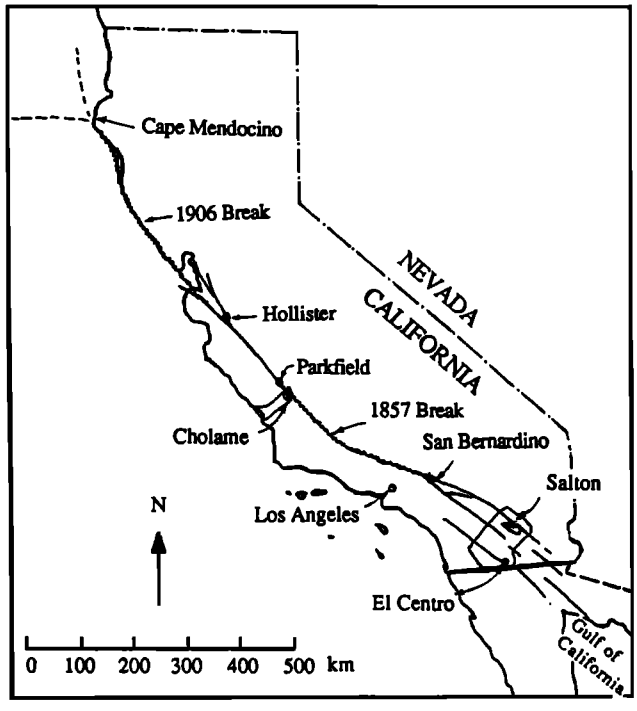

Fig. 1. Map of California with San Andreas fault indicating the geodetic networks covering the region whose surface velocity is studied in this paper [after *Allen*, 1968].

measurements [*Clark et al.*, 1987] crossing the San Andreas and the San Jacinto faults, consistent surface velocity profiles can be generated, although information on the history of great ruptures and plate velocity accommodation on these fault segments are too sparse to place tight constraints on the model parameters. The repeated line length observations for the Salton Sea network has been made by the U.S. Geological Survey (USGS) since the early 1970s. The VLBI measurements were made between 1982 and 1988 as part of the Crustal Dynamics Project operated by the National Aeronautics and Space Administration.

Modeling Procedure

The modeling procedure follows *Li and Rice* [1987]; a synopsis is given here.

The line-spring procedure as adopted in the original base-traction model involves approximating the layered geometry (Figure 2*a*) as a plane containing a line of slip discontinuity (Figure 2*b*) and undergoing plane stress deformation.

For the base-loaded elastic plate the thickness averaged fault parallel (and only nonvanishing) displacement $u(y, t)$ is related to the shear drag $\tau_x(y, t)$ acting on the base of the plate by imposing equilibrium and using the elastic stress-displacement gradient relationship. For the linear viscoelastic asthenosphere the shear drag is connected to the displacement and displacement rate through a Maxwellian relation. The coupling between the lithosphere and asthenosphere is ensured by imposing a continuous displacement u and shear drag τ_x at the interface between the surface plate and the underlying substrate. This procedure follows the generalized Elsasser model [*Rice*, 1980; *Lehner et al.*, 1981], and results in a governing equation for the time and spatial distribution of deformation in the lithospheric plate

$$\left[\alpha + \beta \frac{\partial}{\partial t}\right] \frac{\partial^2 u}{\partial y^2} = \frac{\partial u}{\partial t} - V_0(y) \tag{1}$$

where $\alpha = HGh/\eta$, $\beta = bH = (\pi H/4)^2$ and G is the shear modulus, H is the lithospheric plate thickness, h is the effective elastic depth over which asthenospheric shear takes place, and η is the asthenosphere viscosity. $V_0(y)$ is the rate of motion of subasthenosphere material of the upper mantle such that $V_0(y) - V_0(-y)$ approaches the remote plate velocity V_{pl} as y increases (see *Li and Rice* [1987] for additional remarks on $V_0(y)$). The Elsasser model relaxation time $t_r \equiv \beta/\alpha \approx (\pi^2 H/16h)(\eta/G)$ is essentially a fraction of the relaxation time for asthenosphere material [*Lehner et al.*, 1981].

The second step relates the thickness-averaged values of stress transmitted across the plate boundary to the net slip $(2u - D)$ across the fault by a proportionality constant or line spring stiffness k. Thus the appropriate boundary condition at $y = 0^+$ is

$$G \frac{\partial u}{\partial y} = k(2u - D) \tag{2}$$

The staircase time function $D(t)$ of plate boundary earthquake rupture motion with steps of magnitude Δ and periodicity T_{cy} may be decomposed into a steady motion with velocity equal to $V_{pl}/2$ and sawtooth motion with seismic slip jumps of Δ and the same periodicity, so that $\Delta = V_{pl} T_{cy}$. It turns out that for the transient solution of $\dot{u}$ or $\dot{\tau}_x$ in response to the sawtooth component motion the exact form of $V_0(y)$ is not needed. For cyclically time-dependent solution $u(y, t)$, *Li and Rice* [1987] solved (1) with $V_0 = 0$ subject to (2) with $D(t)$ replaced by the sawtooth motion component at the plate boundary.

The different physical features at the plate boundary can be represented by edge crack strips with appropriate crack geometries. For the single fault modeled by Li and Rice the local plate boundary geometry may be represented by a single crack as shown in Figure 3*a*. A plate margin which exhibits shallow creep behavior can be represented by a colinear double-edge crack strip shown in Figure 3*b* where the lower crack represents the deep aseismic slip zone, the upper crack represents the shallow creeping zone, and the region in between represents the locked zone which remains stationary between great earthquakes. The stiffness k for this geometry [*Tse et al.*, 1985] is

$$k = \frac{\pi G}{2H} \frac{1}{\ln\left[2/[\cos(\pi a/H) + \cos(\pi b/H)]\right]} \tag{3}$$

where a is the length of the lower crack and b is the length of the upper crack. The deeper end of the locked zone is then given by $L = H - a$, whereas the shallower end of the locked zone is given by b.

The presence of two subparallel adjacent faults can be represented by a pair of adjacent edge cracks of sizes a_1 and a_2 separated a distance d apart, as shown in Figure 3*c*. If the faults are closely spaced (1 to $2H$ or less), the surface deformation will reflect the fault interaction using this double-edge crack strip model. The stiffness k for this geometry is not available analytically. However, k can be determined numerically using the solutions available for a single-edge cracked strip loaded by line loads in conjunction with an alternating superposition technique [see *Lim*, 1987]. The main idea in this technique is to simulate the presence of two cracks in the strip by alternately satisfying traction-free boundary conditions at the locations of each crack until convergence of the solution is

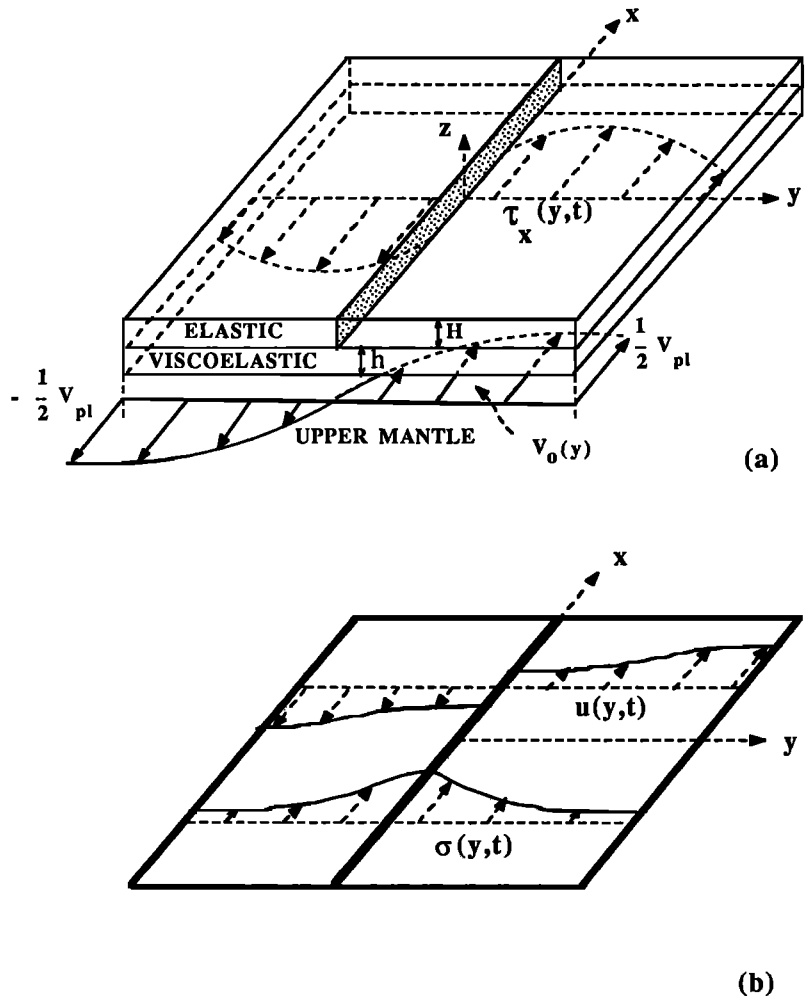

Fig. 2. (*a*) Elastic lithosphere coupled to a viscoelastic asthenosphere driven by upper mantle flow. (*b*) This coupled system is modeled as a (modified Elsasser) two-dimensional plate undergoing thickness averaged deformation $u(y, t)$ and shear stress $\sigma(y, t)$, with a line of slip discontinuity at the fault $y = 0$.

obtained. The stiffness k is given by the remotely applied shear load σ divided by total slip across the crack faces δ where

$$\delta = \delta_{a_1} + \delta_{a_2} = \sum \left[\frac{1}{H} \int_0^{a_1} 2w(y = 0, z)\, dz + \frac{1}{H} \int_0^{a_2} 2w(y = d, z)\, dz \right] \quad (4)$$

The integrands $w(y, z)$ are the displacement (directly proportional to σ) in the x direction for the model shown in Figure 3*c*. In (4) the summation is carried out for the slip contributions from each iteration until convergence of solution is obtained. For the case studied in this paper (where $d \approx H$), convergence is very rapid and only two iterations are required to give an accuracy of 0.1%.

The modeling of the plate boundary as shown in Figure 3 postulates an inelastic constitutive response of essentially constant stress in the shallow creep zone and the deep aseismic slip zone. This has the advantage of deducing rather than imposing the slip displacement in these zones.

The solution of (1) subject to the boundary condition (2) (with the appropriate stiffness k shown in (3) and (4)) follows a procedure similar to that of *Li and Rice* [1987] and yields thickness-averaged values for the lithosphere displacement rates $\dot{u}(y, t)$ and base-traction rates $\dot{\tau}_x(y, t)$.

The surface displacement rate or velocity can be calculated from the thickness-averaged value using an approximation scheme that considers the specific geometry of the system. The surface velocity $\dot{u}_s$ is given in a general form in terms of the thickness-averaged displacement rates as

$$\dot{u}_s = \dot{u} - \dot{u}(y = 0^+)[1 - S(y)] \quad (5)$$

where $S(y)$ is a correction factor specific to the plate boundary geometry (Figure 3). This procedure of approximating the surface displacement rate was suggested by *Li and Rice* [1987] and has been adopted in the original version of the base-traction model involving a single major fault (Figure 3*a*). The procedure was shown to be accurate especially for conditions prevailing at mid to late earthquake repeat cycle times when the basal tractions are not too concentrated near the fault.

The function $S(y)$ is obtained from the surface displacement of the edge-cracked strip subjected to a remotely applied σ. In its general form, $S(y)$ is given by

$$S(y) = F(y)/F(y = \infty) \quad (6)$$

where $F(y)$ is defined by

$$F(y) = \left[u_s(y) - \frac{\sigma y}{G} \right] \quad (7)$$

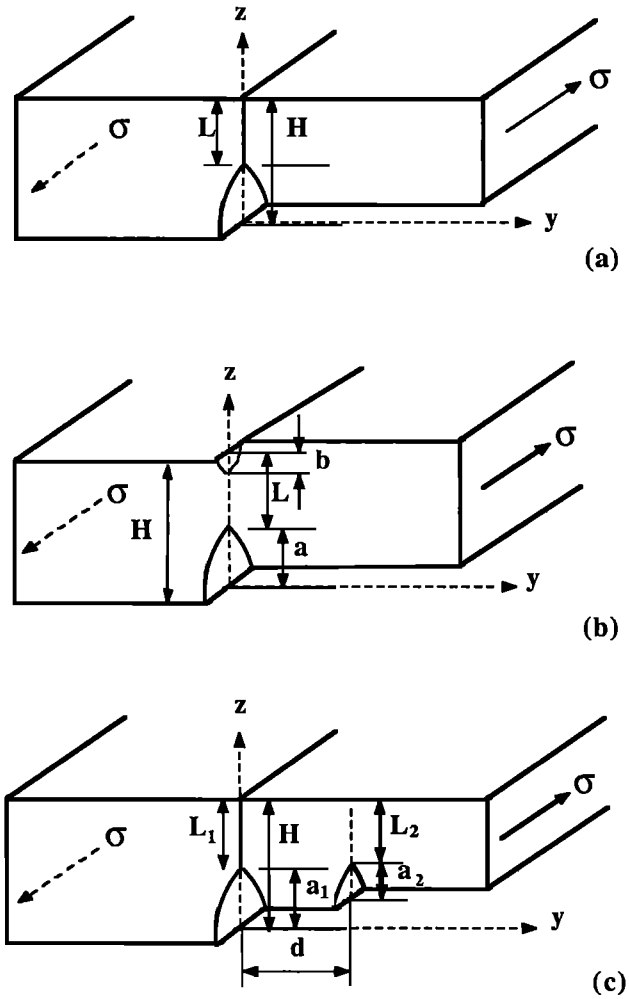

Fig. 3. Three plate boundary models: (*a*) A simple plate boundary modeled with a single-edge crack [*Li and Rice*, 1987]; (*b*) a plate boundary with surface creep modeled with colinear double-edge cracks; and (*c*) a plate boundary with subparallel faults modeled with two adjacent edge cracks.

and an intermediate step involves a translation of the coordinate system such that $F(y = \infty) = F(y = -\infty)$. In essence, $F(y)$ gives the additional displacement due to slip discontinuities at the plate margin over the elastic deformation ($\sigma y/G$). $S(y)$ then controls the normalized distribution factor that smears such deformation onto the ground surface.

For the double-edge crack strip shown in Figure 3*b*, $S(y)$ can be determined analytically. Using (6) and (7) and the known solution for $u_s(y)$ [*Tse et al.*, 1985], $S(y)$ is determined to be

$$S(y) = \frac{\ln [A + \sqrt{A^2 - B^2}] - \ln B - \pi y/H}{\ln [1/B]} \tag{8}$$

where $A = 2 \sinh^2 (\pi y/2H) + \cos^2 (\pi a/2H) + \sin^2 (\pi b/2H)$ and $B = \cos^2 (\pi a/2H) - \sin^2 (\pi b/2H)$.

However, there exists only a numerical solution for the surface displacement of the adjacent double-edge crack strip loaded remotely by σ as shown in Figure 3*c*. In this case, $S(y)$ would have to be computed numerically using (6) and (7).

Surface Velocity at the Cholame-San Luis Obispo Area

The deformation field in the Cholame-San Luis Obispo area could be attributed to both deep aseismic slip and shallow fault creep. Within the framework of the extended base-traction model the earthquake loading process can be described using six parameters, i.e., plate velocity V_{pl}, locked depth L, lithospheric thickness H, cycle time T_{cy}, Elsasser model relaxation time t_r, and the depth of the shallow end of the locked zone b. Our approach is to choose these parameters based on geologic, geodetic, and seismic considerations (independent of the set of data to be compared to) and then to compare the surface velocity from model predictions with that deduced from trilateration measurements [*King et al.*, 1987]. The geodetic subnetwork which provides these field data is shown in Figure 4.

We have set $V_{pl} = 35$ mm/yr based on geologic studies by *Sieh and Jahns* [1984] at Wallace Creek on the Carizzo Plain, approximately 75 km southeast of Cholame. The fault offset data there indicate an average slip rate of 34 ± 3 mm/yr over the past 3700 years. If the nucleation depth for a large earthquake is to be identified with the highly stressed region at the border of the deep slipping and locked zone, [*Li and Rice*, 1987], i.e., with the lower crack tip in Figure 3*b*, then the locked zone depth may be fixed at $L = 9$ km to correspond to nucleation depths of several contemporary earthquakes along the San Andreas fault. For example, the nearby 1966 Parkfield earthquake is inferred to have initiated at about 9 km depth [*Lindh and Boore*, 1981]. However, the nucleation depth of the 1857 rupture is not known. The 9-km depth is near the base of the San Andreas seismogenic zone extending typically to 12–14 km depth from which seismic signals emanate [*Eaton et al.*, 1970; *Wesson et al.*, 1973; *Sibson*, 1982]. The cycle time T_{cy} was chosen to have a range of 145–200 years based on conclusions reached by *Sieh* [1984] using data from extensive trenching at Pallet Creek.

Li and Rice [1987] suggested H and t_r to be 20–30 km and 10–16 years, respectively (corresponding to a viscosity of the lower crust or crust mantle transition zone of $\eta = 2 \times 10^{18}$ to 10^{19} Pa s) based on fitting their model-predicted surface strain rate at the fault trace to the composite time decay strain rate data assembled by *Thatcher* [1983] for the San Andreas fault.

This extended version of the base-traction model introduces a new parameter b which may correspond approximately to the upper depth of microseismic activity. Along the creeping segment of the San Andreas fault in central California, microseismic activity is reported to be concentrated mostly in the 3-

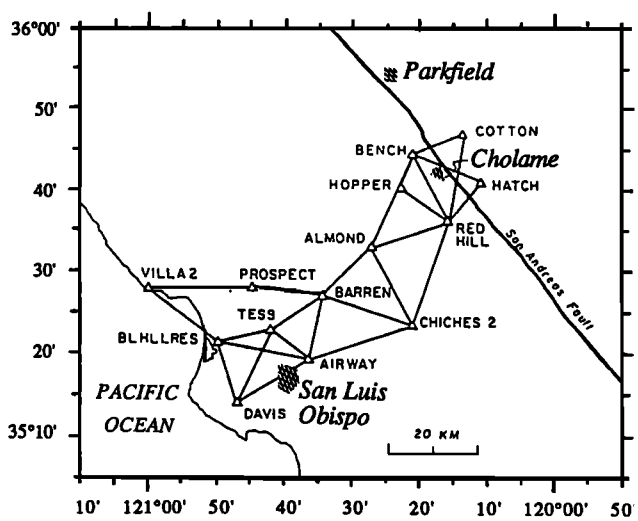

Fig. 4. Geodetic network of the Cholame-San Luis Obispo area [after *King et al.*, 1987].

TABLE 1. Model Parameters for the San Andreas in the Cholame-San Luis Obispo Area

Parameter	Value	Basis	Reference
Lithospheric plate thickness H	20–30 km	composite strain rate along San Andreas over an EQ cycle	*Thatcher* [1983] and *Li and Rice* [1987]
Relaxation time t_r	10–16 years	composite strain rate along San Andreas over an EQ cycle	*Thatcher* [1983] and *Li and Rice* [1987]
Plate velocity V_{pl}	35 mm/yr	geologic studies at Wallace Creek	*Sieh and Jahns* [1984]
Deep locked depth L	9 km	nucleation depth at Parkfield	*Lindh and Boore* [1981]
	8 km	microseismicity map	*Sibson* [1982]
Shallow locked b	3 km	microseismicity map	*Sibson* [1982]
Cycle time T_{cy}	140–200 years	trenching at Pallet Creek	*Sieh* [1984]
Contemporary time t	123 years from 1857		

to 8-km interval [*Sibson*, 1982; *Wesson et al.*, 1973]. Hence b was fixed to be 3 km, as a lower limit. Model predictions were also generated using $L = 8$ km so as to be consistent with microseismicity evidence, but the results were not significantly different from those using $L = 9$ km. Model parametric values discussed in the several paragraphs above are summarized in Table 1.

Figures 5*a*, 5*b*, and 5*c* show the effect on the predicted velocity profiles of varying the parameters H, t_r, T_{cy}, respectively, within the respective ranges indicated above. A contemporary time of $t = 123$ years (1857 + 123 years = 1980) was used, based on the time since the last great earthquake in 1857. These curves do not differ from each other significantly. The far-field velocity approaches $V_{pl}/2 = 17.5$ mm/yr. The predicted surface creep rate of 2.3–3.1 mm/yr indicated by the velocity jump across the San Andreas fault is mainly controlled by b. For the late cycle time ($t = 123$ years, approximately $0.75T_{cy}$ for $T_{cy} = 160$ years) the surface velocity generally increases with a higher relaxation time t_r, a higher cycle time T_{cy}, and a smaller lithospheric thickness H.

For comparisons with geodetic data at the Cholame-San Luis Obispo area [*King et al.*, 1987], we have chosen the set of model parameters common to the solid curves in Figures 5*a*, 5*b*, and 5*c*. This set of parameters is also used by *Li and Rice* [1987] to predict the velocity profile in the Palmdale area. This is probably appropriate since the 1857 great earthquake ruptured both the fault segment near Parkfield and that near Palmdale and if the Earth structure does not change appreciably from Parkfield to Palmdale. The predicted velocity profile is shown in Figure 6 (curve for $b = 3$ km) together with the geodetic data. The model prediction appears to be in general agreement with the field data. The data points near the San Andreas seem to be somewhat underestimated, which suggests the possibility of a greater depth for the shallow end of the locked zone b.

We now consider the predicted and measured creep rate on the San Andreas near Cholame. Surface fault creep of 3.37–4.08 mm/yr at Water Tank (approximately 5 km northwest of Cholame) was measured by creep meters over the period 1969–1980 [*Schulz et al.*, 1982]. A USGS alinement array measures 3.7–4 mm/yr over the 1966–1979 period [*Burford and Harsh*, 1980]. Creep meters span a zone 10–30 m wide, whereas the alinement arrays span a zone up to 200 m wide, so that these measurements may be regarded as a lower limit of what may be a greater total fault creep rate measured over a broader width across the San Andreas. Estimates of surface creep rate at Cholame were also made by means of a small-aperture trilateration network which spans up to 3–4 km over a period of 1977–1985. *King et al.* [1987] reported 3.5–4.6 mm/yr of right-lateral surface creep rate.

The lower and upper bounds of surface creep rates estimated from the creep meter, the alinement array, and the small-aperture network are summarized in Figure 7. Figure 7 also shows the model-predicted values of surface creep rate as a function of b. Comparison between model prediction and field data indicates that a proper choice of b probably fall between 4 and 5 km. The predicted surface velocity profile based on $b = 5$ km is shown as the dotted line in Figure 6. The fit to Figure 6 may further be improved if we chose a slightly greater H ($=25$ km) and higher t_r ($=16$ years), still within the range constrained by Li and Rice, discussed earlier. This is shown as the dashed line in Figure 6.

From the above discussions, we conclude that the Li-Rice base-traction model with the inclusion of a surface creep zone modeled as cracklike slipping region could predict surface velocity profiles and fault creep rates consistent with available geodetic data. We emphasize here that while the model parameters are not tightly constrained, they are in agreement with those used to predict the velocity profile at Palmdale [*Li and Rice*, 1987; M. Lisowski and J. C. Savage, personal communications, 1987] J. R. Rice et al., submitted manuscript, 1988; and also with those used to compute the surface strain rate over the whole earthquake cycle for the San Andreas [*Li and Rice*, 1987].

In spite of the reasonable agreement between model-predicted surface deformation and geodetic measurements, the present model may be expected to suffer from inaccuracy due to the assumption of uniformity along the fault strike. Physically, this is clearly not the case. The locked zone width ($(L-b)$ in Figure 3*b*) probably narrows from Cholame toward Parkfield and disappears altogether in the high creep rate zone (≈ 35 mm/yr) in central California. This geometric three dimensionality has been analyzed by *Tse et al.* [1985], *Stuart et al.* [1985], and *Harris and Segall* [1987], amongst others. However, these models do not address the cyclic stressing of the plate boundary associated with coupling of deformation of the shallow crust to deep steady upper mantle motion, as is done in the present modeling effort. Future improvements may combine these features into a single model.

The data modeled [*King et al.*, 1987] were derived from a solution in which the fault normal component of displacement was minimized. *Harris and Segall* [1987] found that in order to fit trilateration measurements from the San Luis trilateration network, it was necessary to include a component of

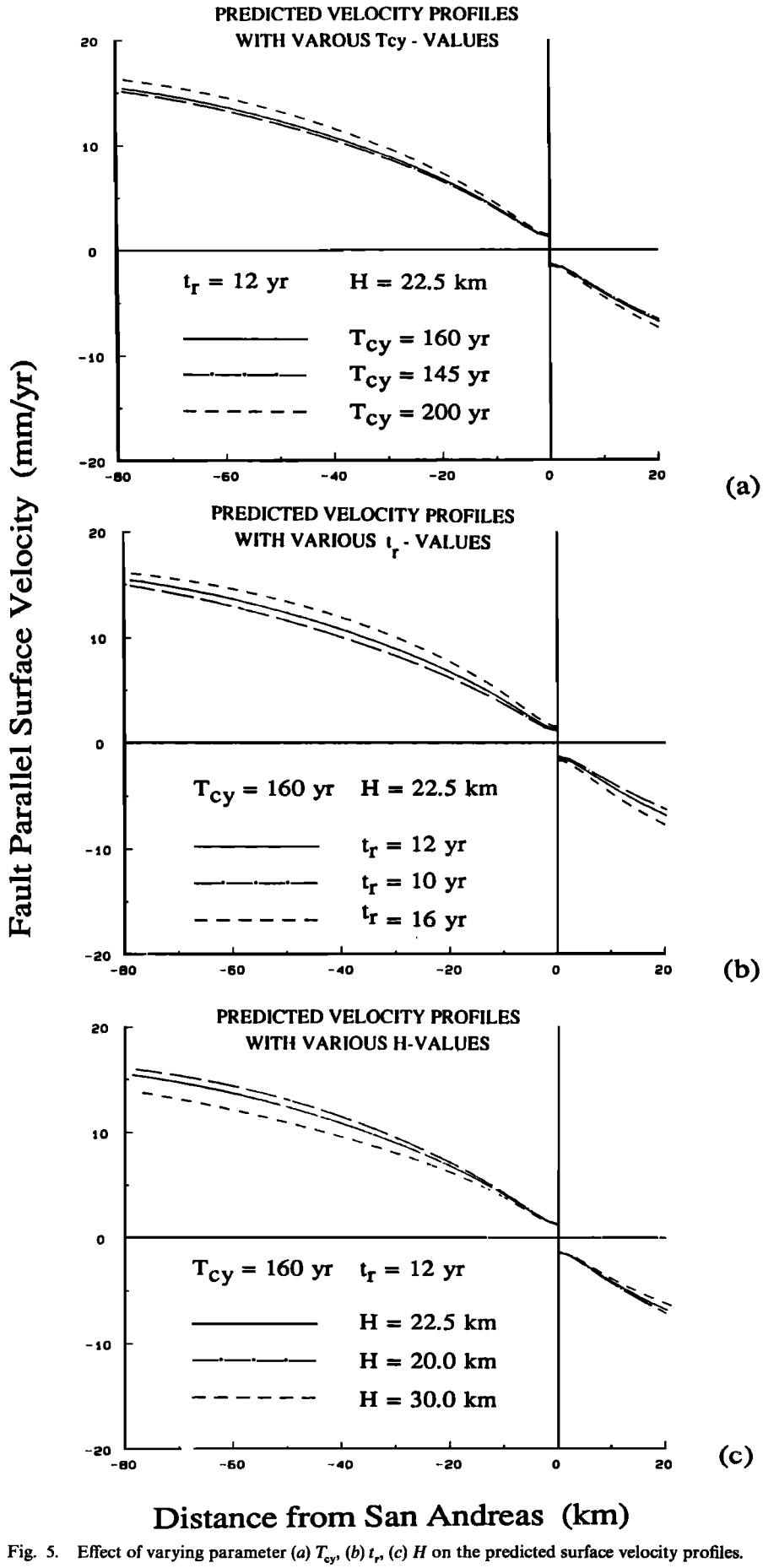

Fig. 5. Effect of varying parameter (*a*) T_{cy}, (*b*) t_r, (*c*) H on the predicted surface velocity profiles.

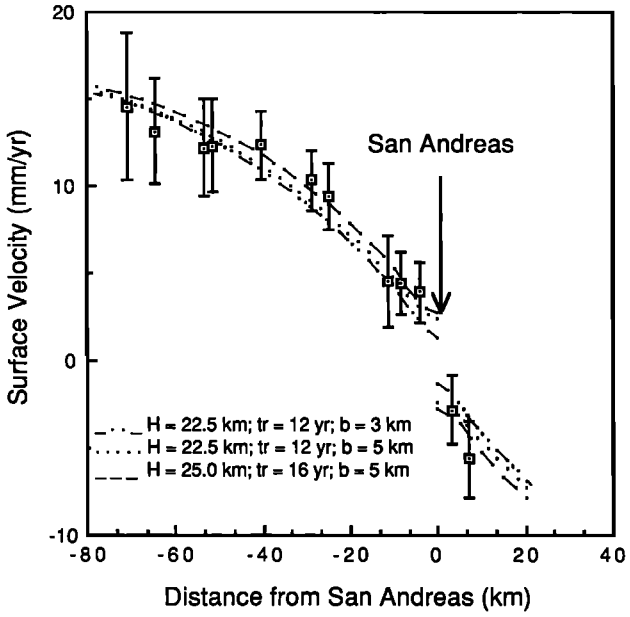

Fig. 6. Comparison of model predicted surface velocity profiles and trilateration data from *King et al.* [1987].

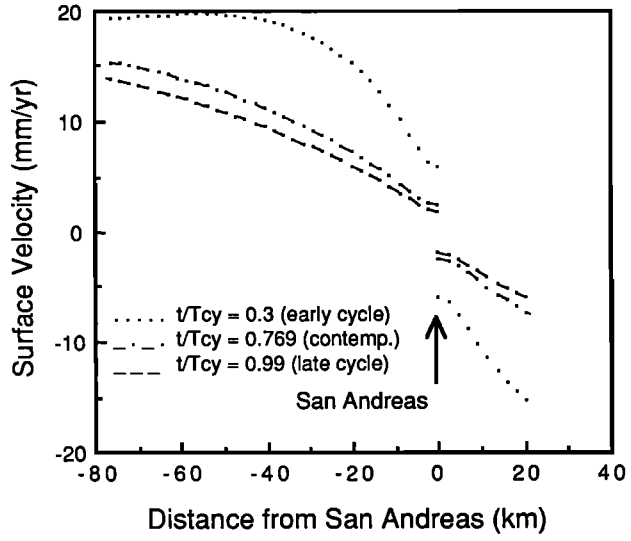

Fig. 8. Model-predicted velocity profiles at three times within an earthquake cycle.

contraction normal to the trend of the San Andreas fault. The estimated compression at a rate of 6.1 ± 1.7 mm/yr, however, may be due to systematic bias in the older trilateration data (J. C. Savage, personal communication, 1987). Even so, there is geologic evidence which reflects compressive behavior normal to the San Andreas in this region (J. Sauber et al., Geodetic measurement of deformation east of the San Andreas fault in central California, submitted to *Slow Deformation and Transmission of Stress in the Earth, Geophysical Monograph Series*, edited by S. Cohen and P. Vanicek, AGU, Washington, D. C., 1988, hereinafter referred to as submitted manuscript, 1988). In addition, the present modeling does not account for the presence of the Riconada fault approximately 40 km west of the San Andreas. This fault has been estimated to accommodate a right-lateral slip rate of 1–2 mm/yr at its northern end (J. Sauber et al., submitted manuscript, 1988).

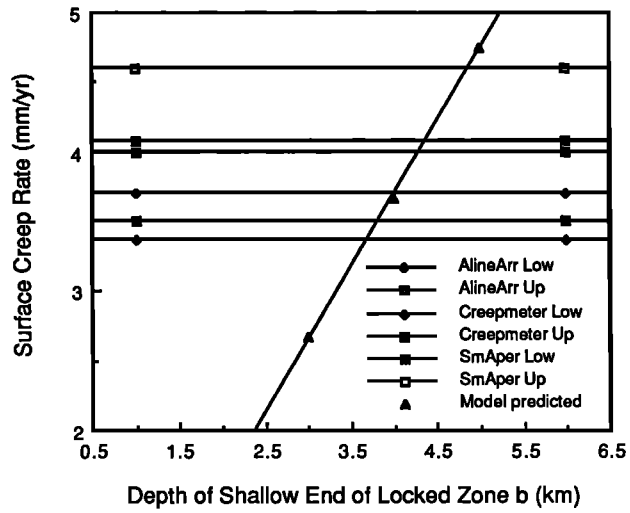

Fig. 7. Horizontal lines indicate the lower and upper bound measured surface creep rates near Cholame by creepmeter (1969–1980 [*Schulz et al.*, 1982]), alinement arrays (1966–1979 [*Burford and Harsh*, 1980]), and small-aperture networks (1977–1985 [*King et al.*, 1987]). Model-predicted variation of surface creep rate with creep zone depth b is superimposed on measurements to indicate the plausible range of b values.

An interesting feature of the present model is that of a locked zone, presumably to be ruptured in the next great earthquake, at a depth between approximately 4 and 9 km. This zone appears to correspond to the depth range where the largest number of aftershocks concentrate following the 1966 Parkfield earthquake [*Eaton et al.*, 1970]. In the aseismic slip zone below the locked seismogenic layer the slip rate increases with depth and averages to approximately 7 mm/yr. This low slip rate is accompanied by a broad distribution of shear deformation due to the base-loading effect.

To study the time dependence of surface deformation, we show in Figure 8 the surface velocity profiles for three times at different portions of an earthquake cycle: 30%, contemporary (≈77%), and at 99% of cycle time T_{cy}. The curves were computed based on the same parametric set as in Figure 6 with $b = 5$ km, $H = 22.5$ km, and $t_r = 12$ years. Figure 8 indicates that the station velocities and fault creep rate may be expected to continue to decrease with time. Unfortunately, the change from contemporary time to the end of the earthquake cycle may be relatively small when compared to the velocity decrease in the early portion of the earthquake cycle, so that the precision of current geodetic measurements may not be adequate to distinguish the contemporary from the end-of-cycle velocity profile.

Surface Velocity at the Salton Sea-Coachella Valley Area

The Salton Sea geodetic network covers an area that is complicated by the presence of the San Jacinto fault (lying 40 km to the west) and the Elsinore fault (lying 70 km to the west) running subparallel to the San Andreas fault (Figures 9*a* and 9*b*). An attempt is made to model the surface velocity profile in this region by means of the adjacent double-edge crack strip (Figure 3*c*) version of the extended base-traction model described earlier in this paper.

The predictions of surface velocity were achieved in the following manner: Separate periodic earthquake sequences involving abrupt slip across the locked zones at the San Andreas and San Jacinto faults could occur such that the surface veloc-

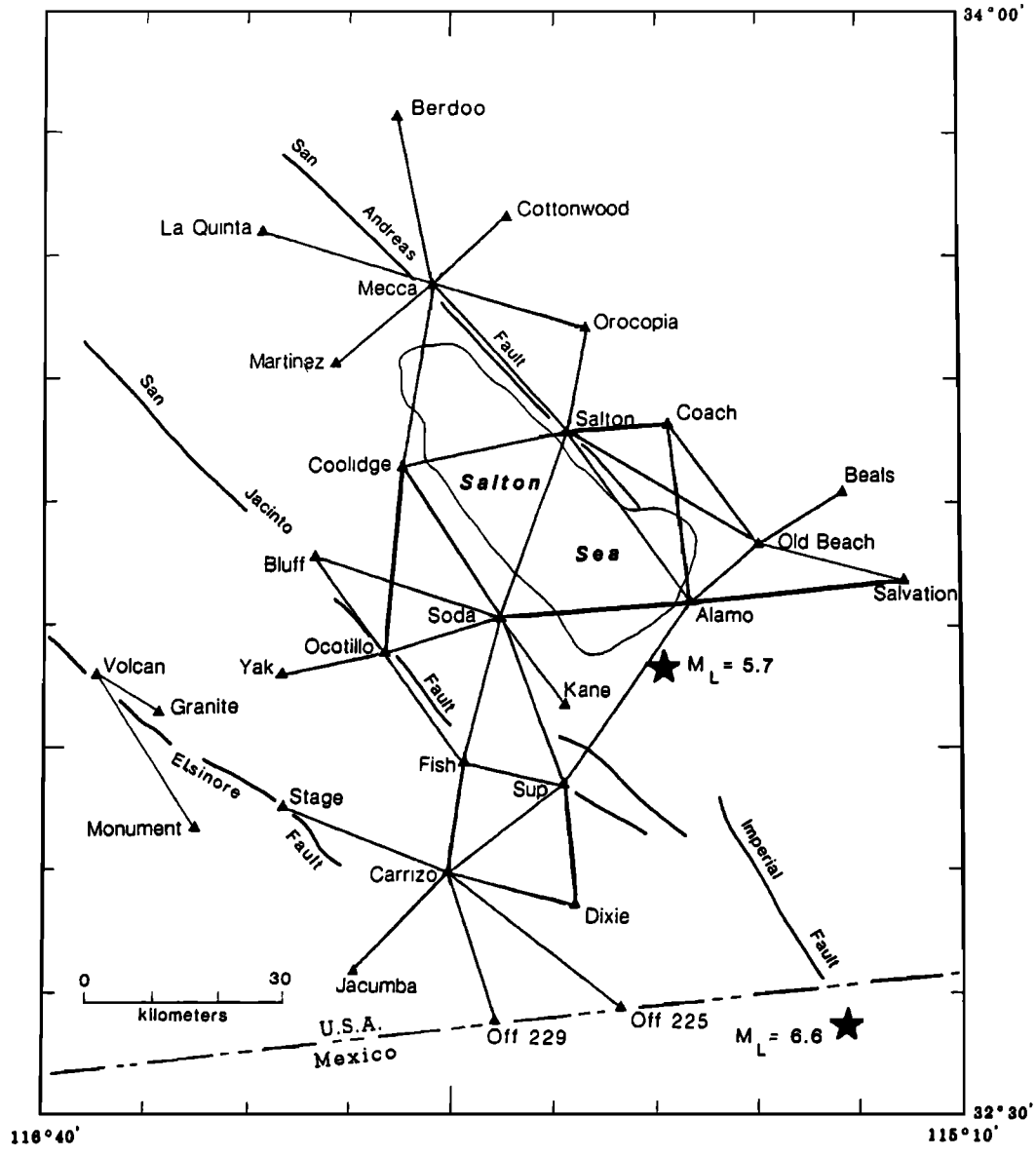

Fig. 9*a*. Geodetic networks covering the San Andreas and San Jacinto faults in the Coachella Valley-Salton Sea area [after *Savage et al.*, 1986].

ity profile is made up of the sum of the velocity profiles associated with these two earthquake sequences. The surface velocity profile for each sequence is obtained from the extended base-traction model using parameters (V_{pl}, L, d, H, T_{cy}, t, t_r) that appear consistent with available geodetic, seismic, and geologic evidence. Tables 2 and 3 show a summary of some seismic and geologic data available to describe the San Andreas and the San Jacinto fault in southern California. It should be noted that the available data do not provide tight constraints on the model parameters. Based on evidence of offset from excavation near Indio, the repeat time T_{cy} for the San Andreas fault was estimated at greater than 600 years [*Sieh*, 1981] and later updated to 200–300 years [*Sieh*, 1986]. The last large rupture was estimated at 300 $\pm$ 40 years [*Sieh*, 1986]. The updated geologic data suggest that the San Andreas in southern California may be reaching the end of an earthquake cycle. For calculation purposes, we have used $t = 0.90T_{cy}$. (Later on, we shall show that a midcycle time might be more appropriate.) Fortunately, the predicted velocity profiles are not very sensitive to t beyond 70% of cycle time [see, e.g., *Li and Rice*, 1987, Figure 3] since the asthenosphere relaxation process is essentially completed by this late cycle time. Table 4 shows three plausible sets of parameters (models 1–3) which we have used in this discussion.

Figure 10 shows the contributions from the earthquake sequences on the San Andreas fault and that on the San Jacinto fault to the predicted total surface velocity profile for model 1. Note that the velocity profiles are only slightly asymmetric about the fault associated with each earthquake sequence. For the thin lithosphere thickness chosen and relatively large distance separation between the San Andreas and the San Jacinto faults ($d/H \sim 2$), the interaction effect is not at all strong.

The model predictions generated with the parameters in Table 4 are compared with the fault parallel station velocities

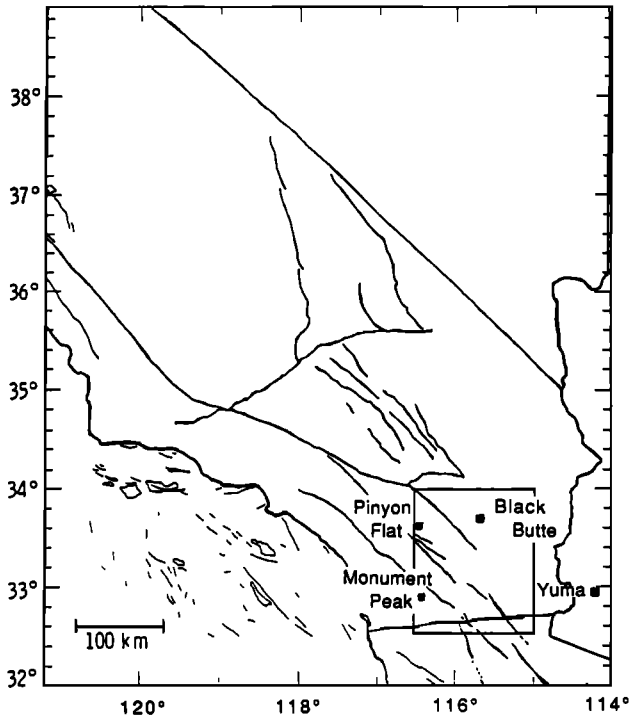

Fig. 9b. Locations of the VLBI sites discussed in this paper. Area of Figure 9a is boxed area.

from trilateration measurements (M. Lisowski and J. C. Savage, personal communications, 1988) and from VLBI measurements [*Clark et al.*, 1987; *Gordon and Sauber*, 1988]. The surface velocity field from trilateration measurements is shown in Figure 11. The VLBI measurements were made with a reference frame fixed on the "stable" North American plate by holding stationary four VLBI sites in Colorado, Arizona, Nevada, and Texas. The stations Monument Peak (MP), Pinyon Flat (PF), and Black Butte (BL) are within the enlarged map of the modeled region shown in Figure 9a. Station Yuma (YU) (Figure 9b) is located southwest of the modeled region. The VLBI data is shown in Figure 12 with error bar given by one sigma. It is seen that this latest derived VLBI data set is quite compatible with the trilateration data.

Comparison of model predicted velocity profile with geodetic data is shown in Figure 12. An arbitrary rigid body translation has been added to the geodetic measurements. For the trilateration data, only the station velocities northwest of the diagonal line shown on the map of Figure 11 are used. This is because of the uncertainty in the fault geometry of the San Andreas and the San Jacinto fault as they approach the northern end of the Imperial fault. The present modeling effort does not account for the presence of the Elsinore fault.

By including the influence of the San Jacinto fault, the model can now account for the general asymmetry of the surface velocity with respect to the San Andreas fault. Model 1 employs most of the model parametric values that have been used for modeling surface velocity profiles in other segments of the San Andreas. The result is not satisfactory, as the predicted profile deviates significantly from most data points. Although a larger velocity accommodated by the San Andreas fault is plausible and would have improved the fit to data, the shape of the predicted velocity profile does not appear to conform to that demanded by the data. Model 2 adjusts the plate thickness H and the relaxation time t_r but still remains within the limits constrained by *Li and Rice* [1987] (see also top two entries of Table 2 or 3). In addition, t/T_{cy} for the San Jacinto fault is reduced to 0.3, and the San Andreas and the San Jacinto faults accommodate higher velocities of 35 and 13 mm/yr, respectively. The predicted profile for this model improves upon that of model 1. It is possible to improve the fit to the data points near Monument Peak by including slip contributions from the Elsinore fault. The apparent best fit to the trilateration data is obtained in model 3, where t/T_{cy} for the San Andreas fault is reduced to 0.5. While this is by no means a systematic parametric study, these modeling attempts together with the geodetic field data appear to suggest that the asthenosphere material has not been fully relaxed in southern

TABLE 2. Parametric Values for San Andreas Fault in Southern California

Parameter	Value	Basis	Reference
Lithosphere plate thickness H	20–30 km	composite strain rate along San Andreas over an EQ cycle	*Thatcher* [1983] and *Li and Rice* [1987]
Relaxation time t_r	10–16 years	composite strain rate along San Andreas over an EQ cycle	*Thatcher* [1983] and *Li and Rice* [1987]
Recurrence time T_{cy}	>600 years	excavation evidence of San Andreas east of Indio	*Sieh* [1981]
	200–300 years	updated excavation evidence of San Andreas east of Indio	*Sieh* [1986]
Plate velocity V_{pl}	11–35 mm/yr	Quaternary data of prehistoric fault offsets	*Crowell and Sylvester* [1979]
	24.5±3.5 mm/yr	Holocene data of fault offsets	*Weldon and Sieh* [1985]
	24±4 mm/yr	analysis of VLBI measurements	*Lyzenga and Golombek* [1986]
	>30 mm/yr	excavation evidence of San Andreas east of Indio	*Sieh* [1986]
Time since last earthquake t	300±40 years (during the period A.D. 1000–1700)	excavation evidence of San Andreas east of Indio	*Williams and Sieh* [1987]

TABLE 3. Parametric Values for San Jacinto Fault in Southern California

Parameter	Value	Basis	Reference
Lithospheric plate thickness H	20–30 km	composite strain rate along San Andreas over an EQ cycle	*Thatcher* [1983] and *Li and Rice* [1987]
Relaxation time t_r	10–16 years	composite strain rate along San Andreas over an EQ cycle	*Thatcher* [1983] and *Li and Rice* [1987]
Recurrence time T_{cy}	~100 years	inferred from slip rate and "normal" 1.2 m for EQ of M_s=7	*Sharp* [1981] and *Wallace* [1981]
Plate velocity V_{pl}	8–12 mm/yr	late Quaternary data of fault offsets (very long term rate)	*Sharp* [1981]
	>5.4 mm/yr	Holocene stream channel offset	*Wesnousky et al.* [1987]
Locked depth L	11 km	hypocentral depth of 1968 Borrego Mountain EQ	*Allen and Nordquist* [1972]
Time since last earthquake t	64 years	historical record (1923)	*Wesnousky et al.* [1987]

California. This does not seem to be consistent with the most recently updated geologic data [*Sieh*, 1986; *Williams and Sieh*, 1987]. However, other interpretations are possible. The asthenosphere relaxation time may be particularly long, the plate thickness particularly thin, or the locked zone much shallower than is expected. If these conjectures are true, they may imply that southern California is tectonically quite different from central and northern California.

The model predictions in Figure 12 are obtained from a superposition of the velocities calculated for each earthquake sequence; hence it is convenient to consider each sequence separately when attempting to study the influence of each model parameter. Also, recall that the surface velocities were obtained from the thickness-averaged velocity using a geometric factor correction scheme. The parameters V_{pl}, T_{cy}, t_r, and t only affect the computation of the thickness average velocities; hence the same conclusions can be made about their influence on the model predictions as those made for the original single-fault version of the model by *Li and Rice* [1987]; namely, the surface velocities are proportional to V_{pl}; the surface deformation is concentrated near the fault trace at early cycle time (low t/T_{cy}), but it is distributed over a progressively broader distance from the fault trace with increasing t/T_{cy}; at early cycle time a lower relaxation time t_r will yield surface velocities that are higher, while at late cycle time, a higher t_r will lead to higher velocities.

The parameters a_1, a_2, and H affect both the computation of the thickness-averaged velocities (through the stiffness k) and the geometric factor $S(y)$. A more compliant system (i.e., higher a_1/H, a_2/H) will yield thickness-averaged velocities which are higher close to the fault trace but still approach $V_{pl}/2$ at a remote distance. Increasing a_1/H (or a_2/H) will also cause increased localization of the surface deformation close to that fault location, and this is incorporated into the geometrical factor $S(y)$. The net effect of increasing a_1/H (or a_2/H) on the surface velocities is to elevate the velocities more sharply at that fault location.

While it is possible to analyze the effect of varying each of the model parameters on the predicted profiles, the loose constraints provided by currently available geologic, geodetic, and seismicity evidence (Tables 2 and 3) do not seem to call for such an analysis at this time.

TABLE 4. Parametric Values Used in Model

Parameter	Model 1	Model 2	Model 3
	San Andreas Fault		
L, km	9	8	8
H, km	22.5	20	20
T_{cy}, years	250	250	250
t/T_{cy}	0.90	0.90	0.5
t_r, years	12	16	16
V_{pl}, mm/yr	30	35	30
	San Jacinto Fault		
L, km	11	10	10
H, km	22.5	20	20
T_{cy}, years	100	100	100
t/T_{cy}	0.5	0.3	0.3
t_r, years	12	16	16
V_{pl}, mm/yr	10	13	10

CONCLUSIONS

We have presented models that incorporate a shallow creeping zone and the presence of two subparallel faults found along certain segments of the San Andreas fault. The model is an extension of the base-traction model originally developed by *Li and Rice* [1987]. The new physical features described

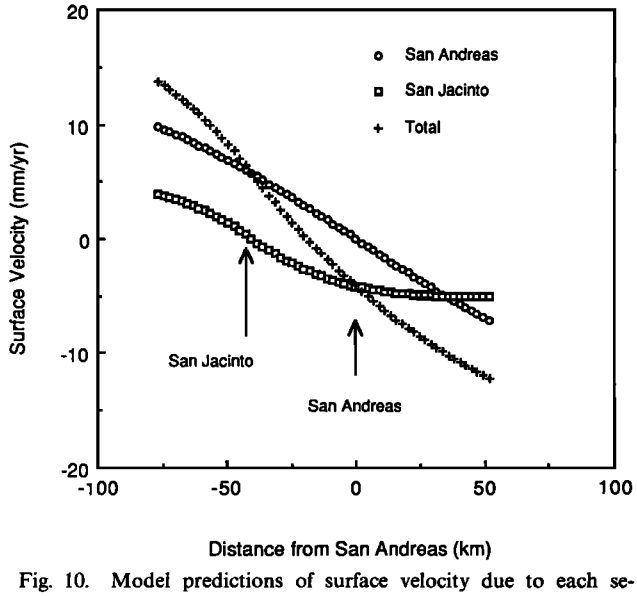

Fig. 10. Model predictions of surface velocity due to each sequence of earthquakes on the San Andreas and on the San Jacinto faults, corresponding to parameters in model 1 (Table 4).

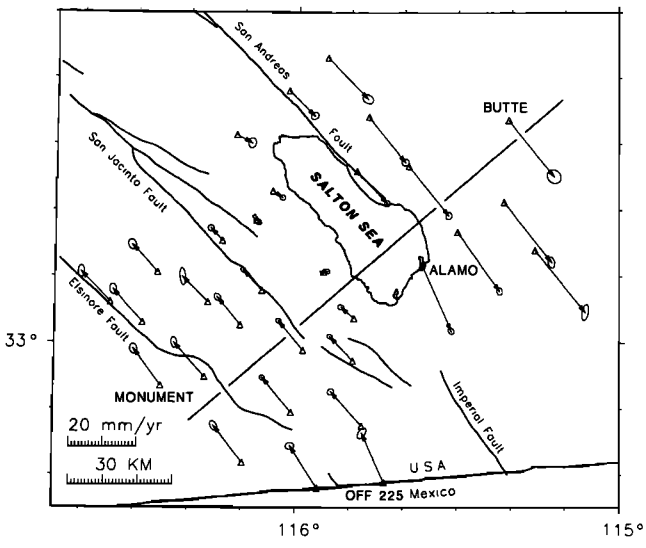

Fig. 11. Surface velocity vectors deduced from trilateration measurements from Salton Sea network (M. Lisowski and J. C. Savage, personal communications, 1988).

above are incorporated into the model by developing the expressions for the plate boundary stiffness and plate boundary surface deformation appropriate to the specific fault geometry.

Model predictions of surface velocity generated using parameters chosen so as to be consistent with geologic, geodetic and seismicity evidence for the Cholame-San Luis Obispo area were found to fit the independent set of contemporary trilateration data [*King et al.*, 1987] reasonably well. The near-fault geodetic data and measured fault creep rates suggest a depth of 4–5 km for the shallow end of the locked zone.

The model which incorporates subparallel faults has been used to generate surface velocity profiles which are compared with geodetic data in the Salton Sea-Coachella Valley area.

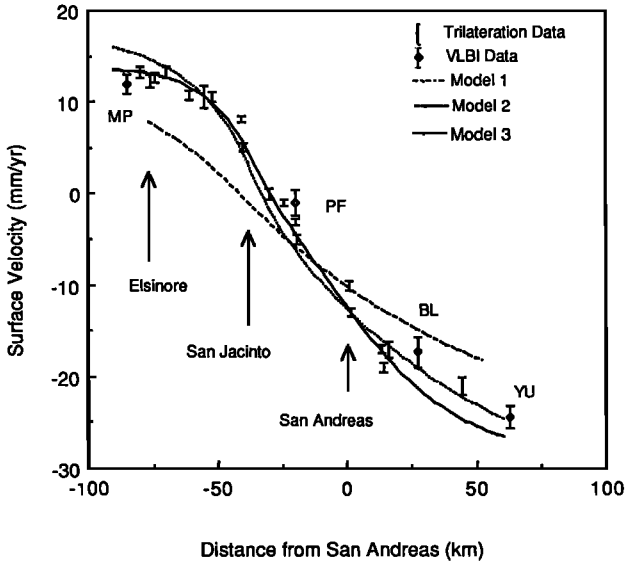

Fig. 12. Comparison of theoretically predicted velocity profiles to trilateration data from M. Lisowski and J. C. Savage (personal communications, 1988) and VLBI data from *Clark et al.* [1987]) and *Gordon and Sauber* [1988] for the three models with parameters shown in Table 4. The VLBI stations Monument Peak (MP), Pinyon Flat (PF), Black Butte (BL), and Yuma (YU) are shown in this figure and in Figure 9*b*.

This model could account for the general asymmetry of the field data with respect to the San Andreas fault and a qualitative reasonable fit to available contemporary geodetic (M. Lisowski and J. C. Savage, personal communications, 1988) and VLBI [*Clark et al.*, 1987; *Gordon and Sauber*, 1988] data could be obtained. However, available geologic, geodetic, and seismicity data do not provide tight constraints on the model parameters. The present modeling results and the contemporary surface velocity from the Salton Sea network do seem to suggest that southern California may be tectonically quite different from central and northern California and that the San Andreas fault there may be in a midcycle rather than in a late-cycle time.

The broadness of the deformation field is found to be controlled by the fault geometry and by the relaxation process of the crust/mantle coupled layers. Multiple subparallel faults spread the deformation over a wider region in comparison to the same amount of fault slip accommodated by a single fault. A larger relaxation time, on the other hand, concentrates shear deformation into a narrower region for a given time in an earthquake cycle. The deformation field in southern California probably reflects these physical constraints.

From these studies we conclude that the Li-Rice model, modified appropriately as in this paper, can provide a reasonable vehicle for studying the loading processes and deformation behavior of plate boundaries with geometric complexities of the sort described here.

Acknowledgments. This work has benefited from helpful discussions with a number of people, particularly, M. Lisowski, J. Sauber, J. Savage, K. Sieh, and R. Stein. M. Lisowski and J. Savage generously provided the unpublished geodetic data for Figures 11 and 12. J. Huang provided able assistance in computations. The authors acknowledge support through a grant to the Massachusetts Institute of Technology from the Crustal Dynamics Program of the National Aeronautics and Space Administration.

REFERENCES

Allen, C. R., The tectonic environments of seismically active and inactive areas along the San Andreas fault system, Proceedings, Conference on Geologic Problems of San Andreas Fault System, edited by W. R. Dickinson and A. Grantz, *Stanford Univ. Publ. Geol. Sci.*, *11*, 70–82, 1968.

Allen, C. R., and J. M. Nordquist, Foreshock, main shock, and larger aftershocks of the Borrego Mountain earthquake, *U.S. Geol. Surv. Prof. Pap.*, *787*, 16–23, 1972.

Bartholomew, M. J., San Jacinto fault zone in the northern Imperial Valley, California, *Geol. Soc. Am. Bull.*, *81*, 3161–3166, 1970.

Bird, P., and R. W. Rosenstock, Kinematics of present crust and mantle flow in southern California, *Geol. Soc. Am. Bull.*, *95*, 946–957, 1984.

Burford, R. O., and P. W. Harsh, Slip on the San Andreas fault in central California from alinement array surveys, *Bull. Seismol. Soc. Am.*, *70*, 1233–1261, 1980.

Clark, T. A., D. Gordon, W. E. Himwich, C. Ma, A. Mallama, and J. W. Ryan, Determination of relative site motions in the western United States using Mark III very long baseline interferometry, *J. Geophys. Res.*, *92*, 12,741–12,750, 1987.

Crowell, J. C., and A. G. Sylvester, Tectonics of the juncture between the San Andreas fault system and the Salton Trough, southeastern California, report, Dep. of Geol. Sci., Univ. of Calif., Santa Barbara, 1979.

Eaton, J. P., M. E. O'Neill, and J. N. Murdock, Aftershocks of the 1966 Parkfield-Cholame California earthquake: A detailed study, *Bull. Seismol. Soc. Am.*, *60*, 1151–1197, 1970.

Gordon, D., and J. Sauber, Geodesy by radio interferometry: Determination and analysis of vector site motions in the southwestern United States, *Eos AGU Trans.*, *69*, in press, 1988.

Harris, R. A., and P. Segall, Detection of a locked zone at depth on the Parkfield, California, segment of the San Andreas fault, *J. Geophys. Res.*, *92*, 7945–7962, 1987.

King, N. E., and J. C. Savage, Strain-rate profile across the Elsinore,

San Jacinto, and San Andreas faults near Palm Springs, California, 1973–81, *Geophys. Res. Lett.*, *10*, 55–57, 1983.

King, N. E., and J. C. Savage, Regional deformation near Palmdale, California, 1973–1983, *J. Geophys. Res.*, *89*, 2471–2477, 1984.

King, N. E., P. Segall, and W. Prescott, Geodetic measurements near Parkfield, California, 1959–1984, *J. Geophys. Res.*, *92*, 2747–2766, 1987.

Lehner, F. K., V. C. Li, and J. R. Rice, Stress diffusion along rupturing plate boundaries, *J. Geophys. Res.*, *86*, 6155–6169, 1981.

Li, V. C., and J. R. Rice, Crustal deformation in great California earthquake cycles, *J. Geophys. Res.*, *92*, 11,533–11,551, 1987.

Lim, H. S., Analysis of elastic crack models under anti-plane loadings and their applications to the study of surface deformations at strike slip plate boundaries, M.S. thesis, Mass. Inst. of Technol., Cambridge, 1987.

Lindh, A. G., and D. M. Boore, Control of rupture by fault geometry during the 1966 Parkfield earthquake, *Bull. Seismol. Soc. Am.*, *71*, 95–116, 1981.

Lyzenga, G. A., and M. P. Golombek, North American-Pacific relative plate motion in southern California from VLBI measurements, *Science*, *223*, 1181–1183, 1986.

McGarr, A., M. D. Zoback, and T. C. Hanks, Implications of an elastic analysis of in situ stress measurements near the San Andreas fault, *J. Geophys. Res.*, *87*, 7797–7806, 1982.

Prescott, W. H., and S. B. Yu, Geodetic measurement of horizontal deformation in the northern San Francisco Bay region, California, *J. Geophys. Res.*, *91*, 7475–7484, 1986.

Prescott, W. H., J. C. Savage, and W. T. Kinoshita, Strain accumulation rates in the western United States between 1970 and 1978, *J. Geophys. Res.*, *84*, 5423–5435, 1979.

Rice, J. R., The mechanics of earthquake rupture, in *Physics of the Earth's Interior*, edited by A. M. Dziewonski and E. Boschi, pp. 555–649, Italian Physical Society/North-Holland, Amsterdam, 1980.

Savage, J. C., W. H. Prescott, and G. Gu, Strain accumulation in southern California, 1973–1984, *J. Geophys. Res.*, *91*, 7455–7473, 1986.

Schulz, S. S., G. M. Mavko, R. O. Burford, and W. D. Stuart, Long-term fault creep observations in central California, *J. Geophys. Res.*, *87*, 6977–6982, 1982.

Sharp, R. V., Variable rates of late quaternary strike slip on the San Jacinto fault zone, southern California, *J. Geophys. Res.*, *86*, 1754–1762, 1981.

Sibson, R. H., Fault zone models, heat flow, and the depth distribution of earthquakes in the continental crust of the United States, *Bull. Seismol. Soc. Am.*, *72*, 151–163, 1982.

Sieh, K. E., A review of geological evidence for recurrence times of large earthquakes, in *Earthquake Prediction: An International Review* edited by D. W. Simpson and P. G. Richards, pp. 181–207, AGU, Washington, D. C., 1981.

Sieh, K. E., Lateral offsets and revised dates of large prehistoric earthquakes at Pallet Creek, southern California, *J. Geophys. Res.*, *89*, 7641–7670, 1984.

Sieh, K. E., Slip rate across the San Andreas fault and prehistoric earthquakes at Indio, California (abstract), *Eos Trans. AGU*, *67*, 1200, 1986.

Sieh, K. E., and R. H. Jahns, Holocene activity of the San Andreas fault at Wallace Creek, California, *Geol. Soc. Am. Bull.*, *95*, 883–896, 1984.

Stuart, W. D., R. J. Archuleta, and A. G. Lindh, Forecast model for moderate earthquakes near Parkfield, California, *J. Geophys. Res.*, *90*, 592–604, 1985.

Thatcher, W., Nonlinear strain build-up and the earthquake cycle on the San Andreas fault, *J. Geophys. Res.*, *88*, 5893–5902, 1983.

Tse, S. T., R. Dmowska, and J. R. Rice, Stressing of locked patches along a creeping fault, *Bull. Seismol. Soc. Am.*, *75*, 709–736, 1985.

Wallace, R. E., Active faults, paleoseismology, and earthquake hazards in western United States, in *Earthquake Prediction: An International Review*, edited by D. W. Simpson and P. G. Richards, pp. 209–216, AGU, Washington, D. C., 1981.

Weldon, R. J., and K. E. Sieh, Holocene rate of slip and tentative recurrence interval for large earthquakes on the San Andreas fault, Cajon Pass, southern California, *Geol. Soc. Am. Bull.*, *96*, 793–812, 1985.

Wesnousky, S. G., C. S. Prentice, and K. E. Sieh, Fault slip-rate determination on the northern segment of the San Jacinto fault, San Bernardino, California, *Eos Trans. AGU*, *68*, 1506, 1987.

Wesson, R. L., R. O. Burford, and W. L. Ellsworth, Relationship between seismicity, fault creep and crustal loading along the central San Andreas fault, Proceedings, Conference on Tectonic Problems of the San Andreas Fault System, *Stanford Univ. Publ. Geol. Sci.*, *13*, 268–274, 1973.

Williams, P. L., and K. E. Sieh, Slow regular slip along the southernmost San Andreas fault for the past 40, 80 and 300 years, *Eos Trans. AGU*, *68*, 1506, 1987.

V. C. Li and H. S. Lim, Department of Civil Engineering, Massachusetts Institute of Technology, Cambridge, MA 02139.

(Received September 4, 1987;
revised March 8, 1988;
accepted November 18, 1987.)